Quantification of deformation microstructure at ultra-low tensile strain in pure Al prepared by spark plasma sintering

Zhang, C. L.; Zhang, Yubin; Wul, G. L.; Liu, W.; Juul Jensen, Dorte; Godfrey, A.

Published in:
I O P Conference Series: Materials Science and Engineering

Link to article, DOI:
10.1088/1757-899X/219/1/012050

Publication date:
2017

Document Version
Publisher's PDF, also known as Version of record

Quantification of deformation microstructure at ultra-low tensile strain in pure Al prepared by spark plasma sintering

IOP Conf. Series: Materials Science and Engineering **219** (2017) 012050 doi:10.1088/1757-899X/219/1/012050

Quantification of deformation microstructure at ultra-low tensile strain in pure Al prepared by spark plasma sintering

C L Zhang[1], Y B Zhang[2], G L Wu[3], W Liu[4], D Juul Jensen[2] and A Godfrey[1]

[1] Key Laboratory of Advanced Materials (MOE), School of Materials Science and Engineering, Tsinghua University, Beijing 100084, China
[2] Section for Materials Science and Advanced Characterization, Department of Wind Energy, Technical University of Denmark, Risø Campus, Roskilde 4000, Denmark
[3] College of Materials Science and Engineering, Chongqing University, Chongqing 400045, China
[4] Advanced Photon Source, Argonne National Laboratory, Argonne, IL 60439, USA

E-mail: awgodfrey@mail.tsinghua.edu.cn

Abstract. A sample of Al with grain size of 5.1 μm, prepared by spark plasma sintering, was deformed to a nominal strain of 0.35% under exposure to X-ray synchrotron radiation, allowing spatially resolved orientation measurements to be made during loading by use of a micro-diffraction technique. A significant heterogeneity in the deformation pattern between grains was observed. A statistical analysis shows that grain deformation depends more on crystallographic orientation than on grain size, with grains with tensile axis lying towards the <001>-<101> border of the unit triangle tending to undergo larger deformation. Other possible reasons for the different deformation behaviour between individual grains are briefly discussed.

1. Introduction

One reason for the continued demand for aluminium alloys as structural materials is the high strength-to-weight ratio of these alloys. To achieve further increases in performance without addition of expensive alloying elements, one solution is through the reduction of grain size into the near-micrometre range, where a good balance between strength and ductility may be possible. There are, however, still some open questions regarding the relationship between material properties and grain size in this regime [1-3]. For a better understanding of the underlying deformation mechanisms in the near-micrometre grain-size regime samples with suitable grain sizes and a simple microstructure are needed for controlled experiments.

Traditionally, fine-grained Al materials have been produced using one of several severe plastic deformation (SPD) techniques. In each case, however, the resulting microstructure is inevitably in a deformed state, with a high dislocation density and a large fraction of low angle boundaries (LABs), and the scope for grain size control in the near-micrometre regime by annealing is limited. Recently, an alternative approach for the preparation of fine-grained samples, namely spark plasma sintering (SPS), has been explored. It has been shown that the SPS technique, originally developed for production of ceramic materials, allows the preparation of metallic samples with controlled grain size, where the grains have a random texture, and are in a fully recrystallized condition, containing a low proportion of LABs [4-6]. This technique is, therefore, well suited for preparation of starting materials for research into deformation mechanisms in the near-micrometre grain-size regime.

Over the last decade, the possibility for non-destructive three dimensional (3D) microstructural characterization has also been realized, and it is been reported that in some cases two dimensional (2D) studies are insufficient [7,8] to reveal fully underlying mechanisms. In this work, we present an in situ experimental study on an SPS-processed Al sample with a 5.1 μm grain size, where the differential aperture X-ray microscopy (DAXM) technique [9,10] is employed for collecting spatially resolved diffraction data from the bulk interior with micrometre resolution. The orientation variations within grains after deformation to near yielding are analysed in detail, and furthermore, the relationships between the grain deformation pattern and both grain size and orientation are also discussed. Additionally, a comparison between 2D and 3D orientation characterization is carried out for one grain, thereby demonstrating the advantage of 3D analysis in revealing clearly the deformation behaviour.

2. Experimental

Pure (99.9%) Al powder with an average powder particle size of 5.7 μm was consolidated by SPS. A maximum sintering temperature of 600 °C and a maximum pressure of 50 MPa were used for the sintering process, the details of which can be found elsewhere [6]. The as-sintered samples have a density of 99% of theoretical density and are in the form of disks with a diameter of 20 mm and a height of 4 mm. Dog-bone tensile specimens were cut from the samples by electron discharge machining. The gauge length, width and height of the cross gauge section of the tensile specimens were 12, 1.8 and 0.6 mm, respectively. Prior to loading, the tensile specimens were mechanically polished and then electro-polished to remove machining damage at the surface.

Synchrotron micro-diffraction experiments were conducted at beamline 34-ID-E at the Advanced Photon Source, Argonne National Laboratory [9]. In the experiment, a polychromatic X-ray beam with energies in the range of 7-30 keV was focused using two non-dispersive Kirkpatrick-Baez mirrors to a size of ~ 0.5 μm. The tensile specimen was mounted on a specially designed tensile device offering a nominal strain resolution of ~ 0.05%, then installed at a 45° incident angle towards the X-ray beam. The diffraction patterns from the X-ray illuminated volume were recorded on a flat panel detector (409.6 × 409.6 mm^2, 2048 × 2048 pixels, and 16-bit dynamic range) mounted in a 90° reflection geometry 510.9 mm above the sample. The detector geometry with respect to the incident beam was calibrated using a strain free silicon single crystal. A Pt wire of 100 μm in diameter was used as a differential aperture for depth-resolution of the Laue diffraction patterns. Reconstruction and indexing of the depth-resolved Laue diffraction patterns were conducted using the LaueGo software at 34-ID-E. Reconstructions were performed to a depth of 150 μm into the sample with a depth spacing of 1 μm. The focused beam was scanned in a 51 × 5 grid at 1 μm step size, resulting in a final 3D data set volume of 51 × 5 × 150 μm^3, with 1 μm^3 voxel size.

Data were collected for the same volume of the sample in both the undeformed state and after tensile deformation to near the yield point (a nominal strain of 0.35%) at a strain rate of ~ 1×10^{-4} /s. The stress at this strain, calculated based on the force measured on a load cell attached to the tensile loading frame, was determined as 55 MPa. In this paper, only results for the deformed sample will be presented.

3. Results and discussion

3.1. Microstructure

The microstructure in the characterized volume after deformation to a nominal strain of 0.35% is shown in figure 1a. After deformation, the grains in the volume are still nearly equiaxed and the orientation variations (seen as colour variations in the figure) within individual grains are very small. Individual grains were identified automatically using a clustering algorithm using a critical angle of 0.2°. In total the examined volume contains 605 grains. The grain size distribution, calculated based on inspection of the centre layer of the mapped volume is shown in figure 1b. The average grain size (calculated as the equivalent area diameter of each grain in this layer) is about 5.1 μm, which matches

well both the starting powder particle size and the grain size measured using electron backscatter diffraction (EBSD) on a similar sample [11]. The sample has a random texture (see figure 1c).

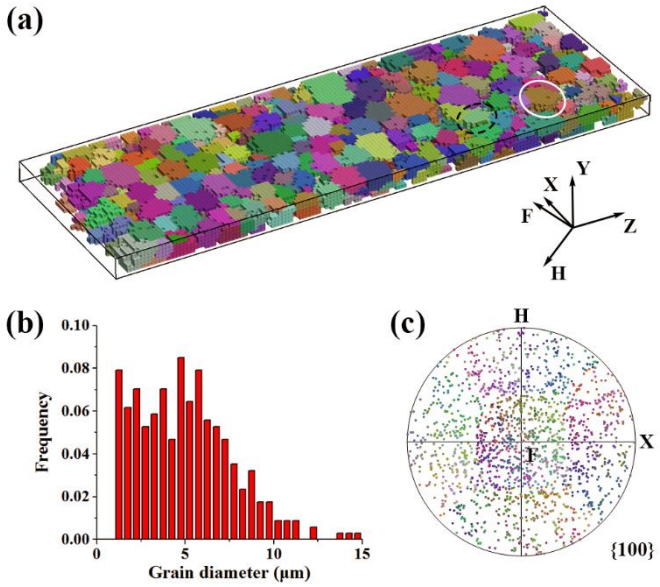

Figure 1. (a) Map (Euler angle colouring) showing the 3D microstructure of the characterized volume (51, 5 and 150 μm along X, Y and Z axis, respectively) after deformation to a nominal strain of 0.35%. The beamline coordinates (X Y Z) and the sample coordinates (X H F) are both defined. The crystallographic orientations are defined in the sample coordinate system. The two grains highlighted by circles are analysed in detail in section 3.2; (b) grain size distribution and (c) {100} pole figure of the characterized volume (colouring corresponding to the grains in (a)).

3.2. Deformation pattern within individual grains

At strain of 0.35%, orientation variations are seen within individual grains. Two grains of similar size chosen for more detailed analysis are indicated by the black-dotted and white-solid circles in figure 1a. As the orientation variation is very small at this strain, typically ~ 0.05°, the orientation data are examined using reference orientation maps based on the grain average orientation after deformation. For these maps the misorientation between each voxel and the average orientation of the grain in which it lies is first calculated in the sample reference frame as an angle:axis pair, and then the results plotted separately for the misorientation angle component (also referred to here as the deviation angle) and the misorientation axis component. It has been shown elsewhere [12] that such maps, in particular the sample-frame misorientation axis map, can be very sensitive to small systematic variations in orientation.

The results are shown in figure 2. For grain G1, an angle deviation of up to 0.2° to the average orientation is seen after deformation (see figure 2a and 3a), and the misorientation rotation axes change gradually and continually from one side of grain G1 to the other side (see figure 2b). In contrast, a different deformation pattern is seen for grain G2. For this grain two distinct regions of different colours are seen in the misorientation rotation axes, implying that grain G2 has subdivided into two parts after deformation.

The distributions of deviation angle to the average orientation for all voxels in grains G1 and G2 are shown in figures 3a and 3c, respectively. An evident difference is seen between the two distributions, which is directly related to the different deformation patterns seen in figure 2. The distributions of neighbour voxel misorientations for the two grains are, however, relatively similar (figure 3b and 3d). The grain orientation spread (defined as the arithmetic mean of the deviation angles between the orientation of each voxels and the average grain orientation) for grains G1 and G2 are 0.08° and 0.07°, respectively, while the grain average misorientation (defined as the arithmetic mean of the misorientation angles between all pairs of nearest neighbour voxels in each grain) is 0.04° for both grains G1 and G2.

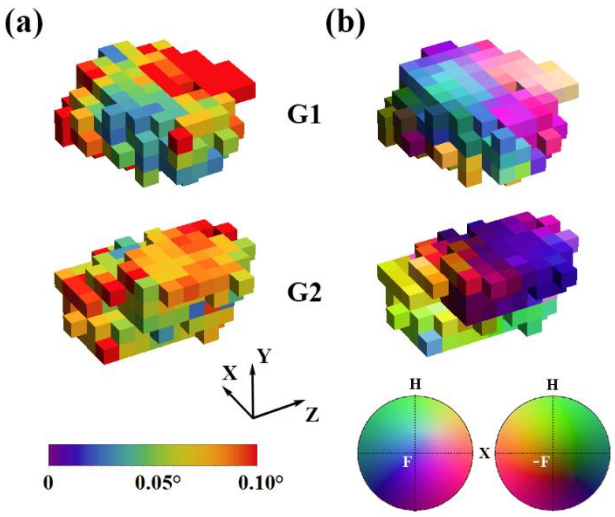

Figure 2. 3D plots of grain G1 and G2 (marked by the white-solid and black-dashed circles, respectively in figure 1a), showing the microstructure after deformation to a nominal strain of 0.35%. The colouring is based on the misorientation between each voxel orientation and the grain average orientation after deformation. (a) Misorientation angle component; (b) misorientation rotation axis component, expressed in the sample coordinate system. The scale bar for the misorientation angle and colour code for the misorientation rotation axis are given.

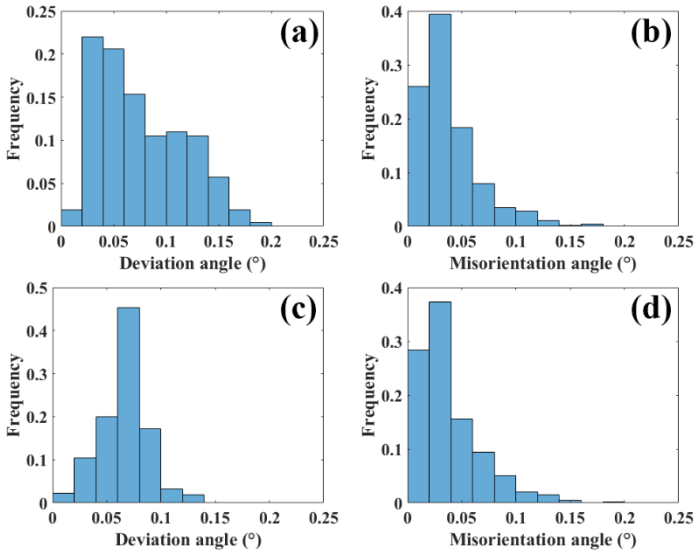

Figure 3. Orientation variation for all voxels in grains G1 and G2. (a) Deviation angle between each voxel orientation and the average orientation for grain G1; (b) misorientation angles between nearest-neighbour voxel pairs in grain G1; (c) - (d) are the corresponding distributions of the two parameters for grain G2.

3.3. Comparison between 2D and 3D measurements

The DAXM technique probes the spatially resolved orientation of the sampled volume, however, most frequently used characterization techniques are performed in 2D. Thus interest arises as to how much difference there is between the 2D and 3D measurements. As mentioned in section 3.1, a layer based analysis from a 3D volume is comparable to an EBSD measurement. In this section, grain G2 is used to demonstrate possible differences between 2D and 3D orientation analysis.

For this demonstration the grain was analysed layer-by-layer. In each layer a calculation was made of the misorientation between the voxel orientations and the average orientation of the grain based only on the measurement in the layer. A quasi-3D data set was then obtained by recombining the data for all layers. For grain G2, the layer based orientation analysis shows smaller deviation angles compared to the volume based result (see figure 4a and 2a), with a mean values of 0.04° and 0.07°, respectively. Moreover, instead of a clearly observed grain subdivision along the Y axis, as seen in

figure 2b, the layer based misorientation rotation axis map shows a weaker more gradual change of orientation, predominantly along the Z axis (see figure 4b).

For a better demonstration of the differences between the 2D and 3D results, a locally magnified view of one pole of a {100} pole figure for grain G2 is plotted by the two methods (see figure 4c and 4d), with the size and colour of each point representing the deviation angle and misorientation rotation axis of the corresponding voxel. A clear difference between the patterns of subdivision can be seen, indicated by the clusters of points with similar colouring, as can the larger deviation angles of the 3D results compared to the 2D analysis. The analysis highlights the fact that 2D data, particularly at low plastic strain and in fine grains, can give misleading or incomplete information about the real pattern of grain subdivision.

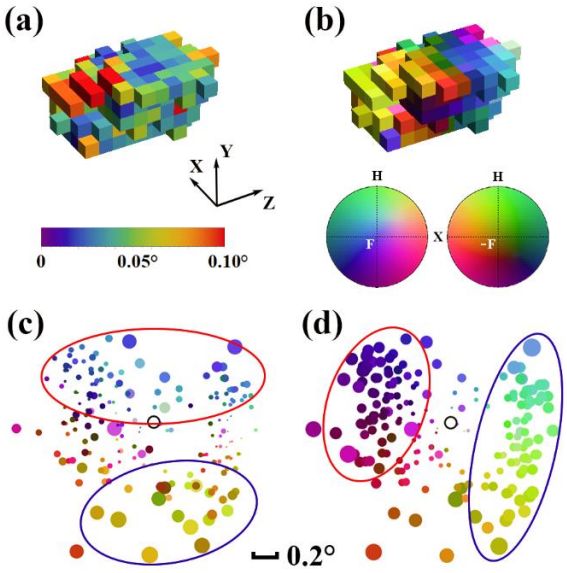

Figure 4. Layer based orientation variation analysis for grain G2 showing (a) misorientation angle component, and (b) misorientation rotation axis (sample coordinate system) component; (c) magnified region of a {100} pole figure, with colouring using the same definition as (b) and where the point size represents the misorientation angle component. The grain average orientation is highlighted by the black circle, and the scale bar corresponds to the point size; (d) corresponding magnified pole figure for the same grain according to the volume based orientation variation result (shown in figure 2). The red and blue circles in (c) and (d) indicate two clusters of voxels with similar colour, i.e. misorientation rotation axis.

3.4. Deformation behaviour of all grains

In order to assess the variation in deformation behaviour for all the grains in the sampled volume, the grain orientation spread and grain average misorientation have been calculated for each grain and are plotted as a function of grain volume in figures 5a and 5b, respectively. A general tendency is seen for larger grains to have a larger grain orientation spread (see figure 5a), although some smaller grains also show a large grain orientation spread. As discussed in [13] this result may arise from a correlation between grain orientation spread and grain size, resulting from the presence of in-grain orientation gradients. In contrast, as shown in figure 5b, the grain average misorientations for large grains are similar to those for small grains, i.e. grain average misorientation does not depend on grain size. The grain average misorientation therefore provides a better estimation of the deformation of individual grains, although it should be noted that the absolute value of this parameter is step-size dependent.

Using this parameter the effect of crystallographic orientation on the deformation has been examined. Figure 5c shows the orientations of the grains having relatively large grain average misorientations (> 0.09°). The figure shows that in general these grains have no preferential orientation. However, it appears that grains with orientations in the lower part of the unit triangle, i.e. in the region towards the <001>-<101> border, have comparatively larger average misorientations than those with orientation close to the <111> corner.

Besides the crystallographic orientation, several other factors may be important for the deformation differences between individual grains, such as the grain shape, the influence of neighbouring grains, and the initial dislocation density in the undeformed state. These factors will be investigated in detail in the future using both experimental and computational (e.g. crystal plasticity finite element modelling) approaches.

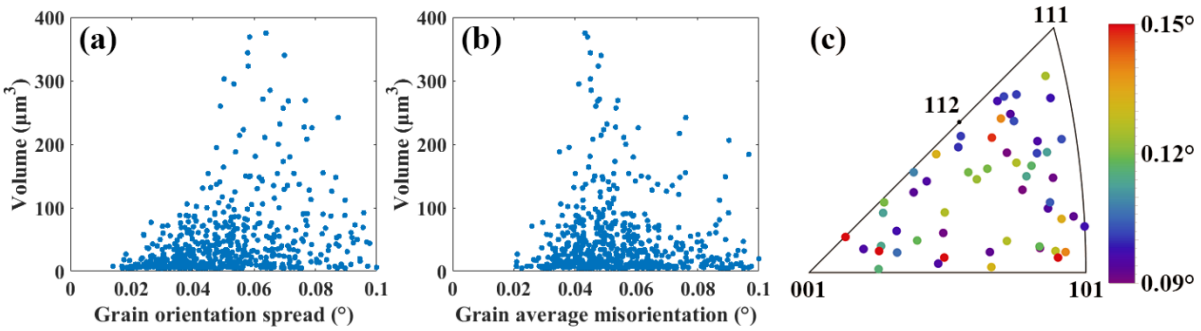

Figure 5. (a) Grain orientation spread and (b) grain average misorientation as a function of grain volume for all 605 grains in the characterized volume. (c) Crystallographic orientations along the tensile direction (H axis in figure 1a) for grains with an average misorientation larger than 0.09°; the colour of each point represents the average misorientation angle of the corresponding grain.

4. Summary

The results show that the 3D X-ray diffraction microscopy technique is a very powerful tool for investigation of deformation microstructure, allowing non-destructive orientation measurements with a spatial resolution of 1 μm and an angular resolution of 0.01°. This combination of characteristics allows for the first time a study of deformation at very low strain in aluminium with near-micrometre grain size. The results show a heterogeneity in the deformation pattern, as quantified by the grain average misorientation. Based on this parameter it is found that grain deformation in this near-micrometre grain-size regime depends more on crystallographic orientation than on grain size, with a weak tendency for grains lying towards the <001>-<101> border of the unit triangle to undergo larger deformation. A comparison between layer based and volume based orientation variation analysis highlights the advantage of 3D measurements for revealing the pattern of grain subdivision.

Acknowledgements

Financial support from the National Natural Science Foundation of China (project numbers 51671113 and 51471095) is gratefully acknowledged. Use of the Advanced Photon Source was supported by the U.S. Department of Energy, Office of Science, Office of Basic Energy Sciences, under Contract No. DE-AC02-06CH11357.

References

[1] Tsuji N, Ito Y, Saito Y and Minamino Y 2002 *Scr. Mater.* **47** 893-9
[2] Hung P C, Sun P L, Yu C Y, Kao P W and Chang C P 2005 *Scr. Mater.* **53** 647-52
[3] Huang X, Hansen N and Tsuji N 2006 *Science* **312** 249-51
[4] Kubota M and Wynne B P 2007 *Scr. Mater.* **57** 719-22
[5] Srinivasarao B, Oh-Ishi K, Ohkubo T and Hono K 2009 *Acta Mater.* **57** 3277-86
[6] Le G M, Godfrey A and Hansen N 2013 *Mater. Des.* **49** 360-7
[7] Lin F X, Godfrey A, Juul Jensen D and Winther G 2010 *Mater. Charact.* **61** 1203-10
[8] Xu C L, Zhang Y B, Godfrey A, Wu G L, Liu W, Tischler J Z, Liu Q and Juul Jensen D 2017 *Sci. Rep.* **7** 42508
[9] Larson B C, Yang W, Ice G E, Budai J D and Tischler J Z 2002 *Nature* **415** 887-90
[10] Larson B C and Levine L E 2013 *J. Appl. Cryst.* **46** 153-64
[11] Le G M, Godfrey A, Hansen N, Liu W, Winther G and Huang X 2013 *Acta Mater.* **61** 7072-86
[12] Hong X, Godfrey A, Zhang C L, Liu W and Chapuis A 2017 *Mater. Sci. Eng.* A **693** 14-21
[13] Delannay L, Mishin O V, Juul Jensen D and Van Houtte P 2001 *Acta Mater.* **49** 2441-51